Composites Part B xxx (2016) xxx-xxx

Contents lists available at ScienceDirect

Composites Part B

journal homepage: www.elsevier.com

Structure and physical-mechanical properties related to comfort of flexible polyurethane foams for mattress and effects of artificial weathering

Paola Scarfato *, Luciano Di Maio, Loredana Incarnato

Department of Industrial Engineering, University of Salerno - Via Giovanni Paolo II, 132 – 84084, Fisciano, SA, Italy

ARTICLE INFO

Article history:
Received 26 July 2016
Received in revised form 21 September 2016
Accepted 16 October 2016
Available online xxx

Keywords:
Polyurethane
Flexible foam
Artificial weathering
Comfort

ABSTRACT

The aim of the work was to test three flexible polyurethane foams for mattress for comfort and durability. In particular, they were investigated the effects of foam composition and cell architecture on some physical-mechanical properties of interest for bedding applications and related to foam comfort levels (i.e. surface firmness, hysteresis loss and resistance to bottoming out), and their changes after artificial weathering due to moisture and temperature.

The results demonstrated that all the three foams have open cell morphology and similar cell structure, with average cell diameters ranging from 430 to 510 micron and wide cell size distribution. As a consequence, they also show comparable water vapor transport behavior. On the contrary, their mechanical response, in terms of hysteresis loss, surface firmness and resistance to bottoming out, was found strongly dependent on their chemical structure and molecular mobility, as inferred from infrared spectroscopy analysis. During accelerated weathering all the foams undergo oxidations that affected their comfort factors in static conditions, giving a progressive lowering of hysteresis loss, surface firmness and resistance to bottoming out, particularly for the two foams having lower crosslinking level and thus slow recovery rate after compression.

1. Introduction

Polyurethane (PU) foams are a class of highly versatile cellular polymers, made up of a solid and gas phase mixed together, industrially produced by polyaddition of polyisocyanates and macropolyols, whereby urethane groups are formed in the polymer backbone (Fig. 1).

Depending on the chemical nature of the reagent molecules, the formulation composition and the reaction conditions, thermoplastic, elastomeric or thermoset PU foams with different morphologies and geometries of their microstructure, and properties tailored for specific applicative fields (building and constructions, transportation, furniture and bedding, packaging, etc.), can be obtained [1]. Among them, open cell flexible PU foams, having low-resilience or 'viscoelastic' behavior, are particularly favorable for applications in several sectors, e.g. bedding, automotive seating, footwear, etc., where high foam comfort levels, as perceived by users, and consistent performance of the foam over its lifetime are required.

Many authors have devoted considerable research efforts on the experimental and theoretical characterization of polymeric foams with the aim to provide insight on the physical-mechanical properties related to the foam architecture and comfort and on their changes during the material normal use, in order to obtain quantifiable variables suitable to measure the foam comfort from the mechanical point of view [2–11]. However, the results are far from conclusive, even because the weathering effects due to environmental agents (such as moisture and temperature) on comfort are only rarely considered. Therefore, more work is still necessary to understand the complex relationships among foam composition, structure, final properties and durability, needful for the design of foam systems able to ensure high comfort levels to users and for the assessment of their lifetime.

In this context, in this work three different flexible PU foams, used as layers in a mattress construction, were analyzed in order to investigate the influence of their composition and architecture (apparent density, porosity, cellular structure) on some physical-mechanical properties related to foam comfort levels (i.e. water vapor permeability, resilience and compression mechanical properties). In particular, with the aim to improve the understanding of factors affecting the foam mechanical comfort in static conditions, stress–strain measurements in 25% and 65% compression and hysteresis tests have been carried out that allowed to highlight the differences in terms of recovery rate, sag factor and hysteresis loss of the analyzed foams. Moreover, since polymers and polymer composites can undergo to some degradation by several environmental agents [12–15], the effects of artificial weathering due to temperature and moisture of the three foams were considered. In particular, accelerated weathering tests, by exposure in a climatic chamber at 50 °C and 95%RH (ASTM D3574) for different time intervals (5, 10 and 15 days), were carried out, in order to investigate the changes in the foam chemical structure and morphology and their effects on the factors affecting the foam comfort.

* Corresponding author.
Email addresses: pscarfato@unisa.it (P. Scarfato); ldimaio@unisa.it (L. Di Maio); lincarnato@unisa.it (L. Incarnato)

http://dx.doi.org/10.1016/j.compositesb.2016.10.041
1359-8368/

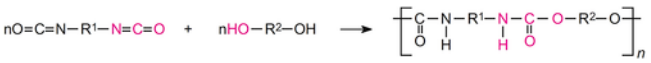

Fig. 1. Urethane linkage formation by reaction between a diisocyanate with a diol.

2. Materials and methods

The study was performed on three commercial flexible polyurethane foams, having different viscoelastic behavior, used as internal components in multi-layer foam mattress fabrication. The materials, commercially named FF60N, VISCOPUR and AP35B, and delivered as of 60 kg/m^3, 45 kg/m^3 and 35 kg/m^3 density, respectively, were kindly supplied by Rinaldi Group s.r.l. (Italy). The foam nomenclature, their position in the mattress structure and their nominal density are reported in Table 1.

All the specimens for the analyses were cut from the blocks of the foamed materials.

The apparent density tests were carried out in accordance with ASTM 3574-03 test A. The value of the apparent density was calculated as the average mass/volume ratio of three regular shaped samples having volume not less than 1000 mm^3.

The cellular structure of the foam samples was evaluated using an optical microscope with video channel. Three micrographs of each foam structure were taken in order to perform the analysis on the basis of more than one hundred cells. The cell average sizes were evaluated analyzing each photo with the IMAGEJ software.

Extraction experiments were carried out on foam samples to compare the level of cross-linking (gel fraction). Small pieces of foams ($20 \times 20 \times 10$ mm^3) were weighed and extracted in N,N-dimethylformamide (DMF) at room temperature for 24 h. The solvent was changed every 8 h. Finally, the solvent was vaporized under vacuum until a stable weight of the specimens was achieved. The percentage of the insoluble portion of the initial sample gave the gel fraction [16].

Equilibrium moisture content was determined as difference between the weight of the foam at equilibrium at 25 °C and R.H. = 50% and the weight of the foam dried under vacuum at 105 °C for 24 h.

Fourier transform infrared (FT-IR) spectroscopy was performed using a Nexus ThermoNicolet spectrometer (Thermo Scientific, USA) equipped with a SmartPerformer accessory for ATR analyses. The samples were scanned 64 times with a resolution of 2 cm^{-1} over the wavenumbers range from 4000 to 650 cm^{-1}. The spectral analyses were performed using an Omnic spectra analyzer.

The water vapor transport behavior through the foam materials was investigated according to the ASTM E 96-93 — Standard Test Methods of Water Vapor Transmission of Materials – Dry Cup Method. About 300 g of silica gel was placed in a glass crystalizing dish, 150 mm diameter and 75 mm deep. The edges of the test specimen, with the same diameter as the dish, were sealed and then mounted air-tight on the dish with silicone rubber. The assembly was then placed in a chamber at T = 25 °C and relative humidity R.H. = 75%. The mass gain of the assembly was recorded periodically and the water vapor transmission (WVT) rate and water vapor permeability (P) were calculated as:

$$WVT = \frac{M}{t \cdot A} \tag{1}$$

where: M is the mass (g) of absorbed water at time t (h) and A (m^2) is the surface of the exposed foam section; and:

$$P = \frac{WVT \cdot h}{P_{(H_2O)} \cdot \Delta\,(\mathrm{R.H.})} \tag{2}$$

where: h(m) is the sample thickness, P(H_2O) = 23.76 mmHg is the water's saturated vapor pressure at 25 °C and Δ(R.H.) = 0.75 is the difference between the R.H. values (expressed as a fraction) at the two sides of the foam sample [17]. Three specimens of each sample were used for the measurements and the average data were reported.

Differential scanning calorimetry (DSC) measurements were performed with a Mettler DSC 822 calorimeter (Mettler-Toledo, USA). The thermograms of 8–12 mg samples, sealed in standard aluminum pans, were obtained by heating the materials at 50 °C/min from −120 °C to 220 °C under a nitrogen gas purge.

The mechanical hysteresis loss (HL) (ASTM D3574-03 X6) of the samples was measured using $200 \times 200 \times 50$ mm^3 foam samples in the compression mode on a SANS CMT 6000 Series testing machine (MTS, China). Each sample was preconditioned by deforming it twice to 75% of its initial thickness, at a rate of 240 mm/min, after which they were allowed to relax for 6 min, without any applied load. After the samples were compressed to 75% of their initial thickness at 50 mm/min, then the compression force was removed at 50 mm/min until the platen fully returned. The HL was calculated as:

$$HL = \frac{\text{Loading Energy} - \text{Unloading Energy}}{\text{Loading Energy}} \times 100 \tag{3}$$

where the Loading Energy is the energy (i.e. the area under the force/deflection curve) required to compress the material to 75% preset deflection (compression cycle) and the Unloading Energy is the energy recovered when the compression platen is retracted from the preset deflection and completely unloaded (decompression cycle).

All the flexible foams were subjected to the indentation force deflection test (IFD) (ASTM D3574-03 B1) on the same SANS machine used in the HL test. Samples ($200 \times 200 \times 50$ mm^3) were preconditioned as mentioned earlier in the hysteresis test. The samples were compressed to 25% of their initial thickness at 250 mm/min under a load of 4.5 N and held in that deformed state for 1 min. The stress on the samples in this state (i.e. 25% deformation after 1 min) was reported as the 25% IFD value. The samples were then further compressed to 65% of the initial sample thickness at 250 mm/min under a load of 4.5 N and held in that deformed condition for 1 min (65% IFD). The sag factor (SF) was calculated as the ratio of 65% IFD to 25% IFD.

Accelerated aging tests were performed according to ASTM D3574-03 Aging Test L - Wet Heat Aging, using an environmental chamber Challenge ACS CH250 (Angelantoni, Italy), which pro-

Table 1
Sample nomenclature and density.

Sample	Mattress structure		Nominal density [kg/m^3]
FF60N	Top comfort layer		60
VISCOPUR	Middle comfort layer		45
AP35B	Bottom core layer		35

vided constant temperature and humidity control. The foam specimens were exposed at 50 °C and 95% R.H. for several time intervals up to 12 days, and the changes in their properties were measured.

Colorimetric analyses were carried out with a CR-410 HEAD colorimeter (Konica Minolta Sensing, Inc.). The color changes were evaluated by the L* (lightness), a* (redness), b* (yellowness) system (ASTM D-1925, CIE 1976) and by the ΔE* total color change [18].

3. Results and discussion

In order to obtain information about the apparent density, the microstructure (i.e. cell structure, pore size and distribution) and the chemical composition of the three foams selected for the study, all materials were preliminarily characterized.

Fig. 2 shows the optical microscopy images taken on the surfaces of the three foams selected for the investigation, and Table 2 reports, for each foam, the values of average pore size and distribution, apparent density and gel fraction. It can be seen that all the samples have an open cell structure. The cells are irregular polyhedral with average diameters of the pores ranging from 430 to 510 μm and large size distributions in all cases. Moreover, the FF60N and VISCOPUR foams have density values near one each other and significantly higher with respect to the AP35B foam, and lower amount of gel fraction, i.e. higher weight fractions of extractables. This suggests that not all of the polyol material is covalently bonded into these two foams.

Fig. 3 compares the FTIR spectra of the investigated materials in the spectral ranges of 3700–2400 cm^{-1}, 1800-1400 cm^{-1} and 1250-950 cm^{-1}. The peak assignments are listed in Table 3, accordingly to the literature [19,20]. All spectra show the characteristic peaks related to urethane linkages, as expected, and are made from aromatic isocyanates, as indicated by the absorption bands at ca. 1597 cm^{-1} and 814 cm^{-1}, due to the presence of aromatic moieties in the foam formulations. Only minor differences are observable among the analyzed foams, markedly: (1) in the intensity of the O—H stretching peak, related to the amount of absorbed water, which decreases progressively in the order VISCOPUR > FF60N > AP35B; and (2) in the amide I carbonyl absorption band (absorptions in the 1600-1800 cm^{-1} region), which is a highly complex vibration mode particularly sensitive to the specificity and the magnitude of the hydrogen bonding. In all cases the peak at 1724-1712 cm^{-1}, corresponding to C═O stretching, is splitted in two parts due to non-bonded hydrogen groups at higher frequencies and to hydrogen-bonded groups at lower frequencies. However, the intensity of the higher frequency absorption is lower in the case of AP35B, indicating a higher amount of hydrogen-bonded C═O groups in this foam. The AP35B spectrum shows also a more intense broad signal at ca. 1660 cm^{-1} (which appears as a shoulder in the VISCOPUR spectrum) assigned to urea ν(C═O) carbonyls, which are able to form strong bidentate hydrogen bonds serving as physical cross-links. These findings suggest that AP35B should have a higher content of rigid segments along the chains, with respect to the other two foams. On the other hand, the shift of the C—O stretching vibrations towards progressively lower wavenumber (1093-1091-1085 cm^{-1}) in the order AP35B > FF60N > VISCOPUR indicates that more C—O—C groups are involved in hydrogen bonding in the last two samples.

The water vapor transport behavior of the foams was investigated by means of a steady-state weight gain method. Fig. 4 shows the moisture gain by the three investigated foams, measured at 25 °C under a Δ(R.H.) = 0.75. The curves evidence that the foam weight gains in the early phase of the experiments (up to ca. 1 h) were substantially faster than later time points. The fast rate of the phenomenon in the early stage of the test can be attributed mainly to sorption of water by the foams, whereas its slower rate in the later time points, when a steady state permeation occur, indicates that sorption by the foam material has reached equilibrium under the test conditions. The water vapor transmission rate and permeability, evaluated from the slope of the linear weight gain profiles of the different foams, are reported in Table 4. The small differences in the water vapor permeability and transmission rate values have to be reasonably related to the different density and molecular structure (polarity, degree of crosslinking, etc.) of the three samples.

Fig. 5 gives the results of the differential scanning calorimetry measurements on the FF60N, VISCOPUR and AP35B foam samples. It can be seen that the glass transition temperatures (Tg) of the foams ranges from ca. −60 °C to 30 °C. The Tg temperature interval is broad for the FF60N and VISCOPUR foams and sharp for the AP35B one, indicating a lower heterogeneity of the last sample [21]. This may be due to the use of lower molecular weight polyols in the AP35B formulation that accounts for more hydrogen bonding between the urethane groups, coherently with the FT-IR results and similarly to other literature findings [22]. The melting peak of FF60N sample in the temperature range 40–70 °C may be due to polyol crystallinity, whereas the large endothermic peaks, centered at ca. 100 °C and 80 °C for the VISCOPUR and AP35B foams, respectively, can be attributed to melting of nonideally-packed NH…C═O hard segment portions adjacent to the soft segment. This type of structural feature could occur in the interfacial zone between the hard and soft phase, as suggested in literature [23–25].

With the aim to get information about the mechanical behavior of the three foams under compression, and about their ability to be soft and supportive, compression load relaxation experiments have been performed according to ASTM D3574-03.

Fig. 6 reports the stress-strain curves of the loading-unloading cycle performed during the hysteresis loss tests for the three foams. All the samples have the typical behavior of foams subjected to compression. Three regions, each dominated by a different deformation

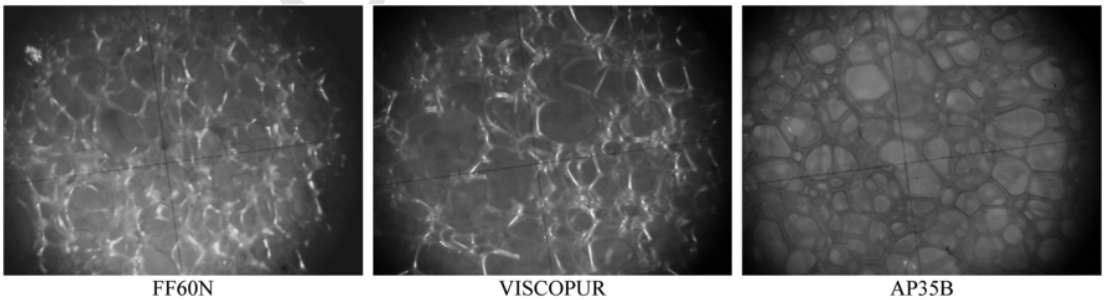

Fig. 2. Optical microscopy images taken (50 X) on the surfaces of the FF60N, VISCOPUR and AP35B foam samples.

Table 2
Average pore diameter (D), apparent density and gel fraction of the FF60N, VISCOPUR and AP35B foam samples.

Sample	FF60N	VISCOPUR	AP35B
D [micron]	430 ± 110	510 ± 130	450 ± 130
Apparent density [kg/m^3]	51 ± 2	48 ± 2	41 ± 1.6
Gel fraction [%]	79.3	94.5	99.1

mechanism, can be identified in the graphs: (i) a first region at low strains where the foams have a linear elastic response, (ii) a second region at medium deformations with a long plateau caused by the cell wall buckling, and (iii) a third region at higher strains in which the stress rises steeply as a consequence of densification phenomena, which start when the opposite faces of the cells touch each other. However, the mechanical hysteresis loss (HL), which is the amount of energy dissipated during the cycle and is a measure of the energy consumption while moving, is markedly different among the three samples, as it comes out comparing the data reported in Table 5. As expectable, the HL, which is related to breakdown and reformation of the mesophase domains (plastic deformation of the hard domains, irreversible disruption of the microstructure, irreversible orientation, etc.) during cyclic deformation, is the lowest in the case of the elastic AP35B foam and is significantly higher for the two viscoelastic FF60N and VISCOPUR foams, where more molecular and microstructural rearrangements are possible. Moreover, whereas the AP35B elastic sample shows a complete recovery of the applied deformation at the end of the test, both the two FF60N and VISCOPUR viscoelastic samples have a residual deformation (6.9% and 5.7%, respectively), which is an indication of increasing relaxation times for these foams, coherently with the FT-IR analysis that demonstrated their higher molecular flexibility. They also show a lower dependence of the stress from the strain, which contributes to a more uniform pressure distribution when the foam is in contact with the body.

Table 5 also reports the values of 25%IFD, which is a measure of the surface firmness, and sag factor SF, which is related to the ability of flexible foams to support load at different indentation levels and gives an indication of cushioning quality. Whereas the 25%IFD value of AP35B is typical of foams conventionally used for mattresses of medium firmness (25%IFD = 25–30%), those of FF60N and VISCOPUR are very low and are indicative of foams with super-soft surfaces. The SF values increase in the order AP35B < FF60N < VISCOPUR, denoting a progressively higher resistance of the foam to bottoming out as the load is applied and then a progressively higher ability to distribute body weight and reduce pressure to the skin.

In order to evaluate the effects of environmental agents (moisture and temperature) on the structure and the properties of the three foams, the samples were submitted to artificial weathering by exposure at 50 °C and R.H. = 95% for different time intervals in a climatic chamber.

With respect to the sample morphology, no cell structure modifications were detected by microscopy observations in all cases. However, colorimetric analysis results, reported in Table 6 as net increase of the total color difference ΔE* respect to the corresponding not weathered foam at different weathering times (t = 1, 3, 6 and 12 days), point out in all cases an increase in the ΔE* values during the weathering. The change is low and remains undetectable to the naked eye (ΔE* < 3) for the AP35B foam, whereas is noticeable for the FF60N and even more for the VISCOPUR ones. These findings are a direct indication of the occurrence of oxidative degradation mechanisms, evidenced also by FTIR analyses, which lead to the color change of the foams.

The FT-IR spectra of the investigated materials, collected before and after 12 days of weathering, in the spectral ranges of 3700–2400 cm^{-1}, 1800–1400 cm^{-1} and 1250–950 cm^{-1}, are compared in Fig. 7. After weathering, it was observed a slight decrease of the bands attributed to the C—H stretching vibrations domain at 3000–2800 cm^{-1}, more evident for the AP35B and FF60 foams and a strong reduction of the C—O—C stretching vibrations at ca. 1090 cm^{-1} in all samples, as a consequence of the oxidation of the polyether soft segments [20]. Moreover, in the case of AP35B and VISCOPUR there is also a decrease of the absorption bands of the urethane function, i.e. the urethane C═O (1724–1712 cm^{-1}), the amide II at 1537 cm^{-1} and the amide III at 1232 cm^{-1}, which may be related to decarboxylation of urethane groups.

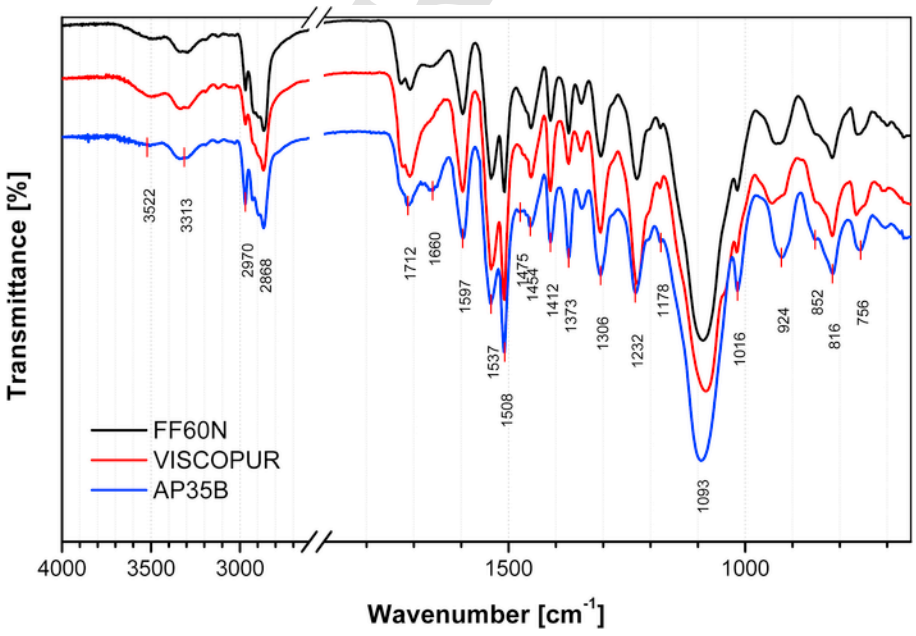

Fig. 3. Comparison among the FT-IR spectra of the FF60N, VISCOPUR and AP35B foams.

Table 3
Frequencies and vibrational assignments of the main peaks in the FT-IR spectra of the FF60N, VISCOPUR and AP35B polyurethane foams.

Wavenumber [cm-1]	Bond	Vibrational modes
3500	O—H	Stretching
3336–3305	N—H	Stretching
3120	C—H (aromatic)	Stretching
2970–2868	C—H (methyl and methylene)	Asymmetrical and symmetrical stretching
1724–1712 (Amide I band)	C═O (urethane, nonbonded and H-bonded)	Stretching
1660 (Amide I band)	C═O (urea)	Stretching
1597	C═C (aromatic ring)	Stretching
1537–1508 (Amide II band)	C—N—H (urethane)	N–H bending + C–N stretching
1475–1454 (Amide II band)	C—N—H (urea)	N–H bending + C–N stretching
1412–1344	C—H (methylene)	Bending and wagging
1306	C—N (urethane)	Stretching
1232 (Amide III band)	C—O—C (ether)	Asymmetrical stretching
	N—H	Bending
	C—N	Stretching
1178	C—H	Wagging
1093–1085	C—O (urethane and ether group)	Stretching
1016	C—H	Symmetrical stretching

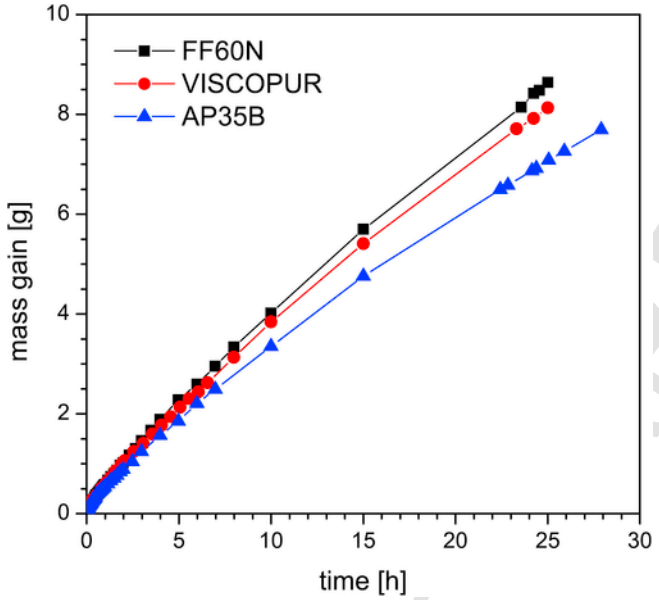

Fig. 4. Mass gained by the FF60N, VISCOPUR and AP35B foams during the test for the water vapor transmission – dry cup method (ASTM E 96-93), at 25 °C.

Table 4
Water vapor permeability (P), water vapor transmission rate (WVT) and equilibrium moisture content (EMC) for the FF60N, VISCOPUR and AP35B foam samples.

Sample	P [g/(mmHg × m × h)]	WVT [g/(m^2 × h)]	EMC [%]
FF60N	0.037 ± 0.001	23.3 ± 1.0	1.28 ± 0.08
VISCOPUR	0.038 ± 0.001	22.8 ± 0.1	1.41 ± 0.06
AP35B	0.032 ± 0.001	19.5 ± 0.2	0.89 ± 0.10

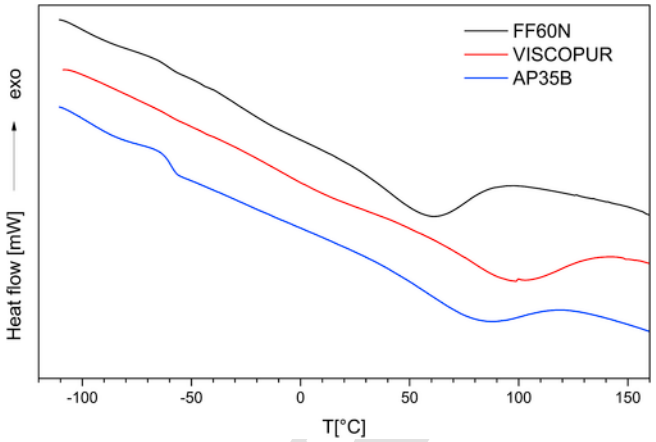

Fig. 5. Differential scanning calorimetry curves for the FF60N, VISCOPUR and AP35B foams.

In all cases no noticeable shift in the N—H (3305 cm^{-1}) and C═O (1712 cm^{-1}) bands can be observed, suggesting that no significant changes in hydrogen bonding occurred.

The evolutions in the FT-IR spectra are coherent with the results of the DSC and colorimetric measurements after artificial weathering. The DSC curves of the weathered foams, shown in Fig. 8, evidence in all cases a decrease of the endothermic peak related to the melting of the hard domain structures (polyol crystals and urethane hard segments).

With the aim to investigate the effect of weathering on the mechanical behavior of the foams, which are very sensitive to molecular recombinations (crosslinking, chain scission) caused by oxidation reactions, as well as to microphase rearrangements (changes in crystallinity, state of organization of the hard and soft segments, etc.) and loss of volatiles (water, plasticizers) occurring during the ageing, all samples were submitted to compression tests.

Fig. 9 reports the stress-strain curves of the loading-unloading cycle performed during the hysteresis loss tests for the three foams, at different aging time intervals. Again, the weathering does not affect significantly the behavior of the AP35B foams, but gives a progressive softening of the FF60N and VISCOPUR ones. These two foams, in fact, show a lower strain-dependence of the loading portions of the hysteresis curves, similar to what would be observed reducing the strain rate of the test. The unloading curves, on the contrary, are nearly identical, indicating that the unloading behavior has less time dependence than the loading one. As a consequence, respect to the corresponding not weathered samples, both the FF60N and VISCOPUR weathered for 12 days (T = 50 °C and R.H. = 95%) show a decrease of about 27% in their HL values, as reported in Table 7. Since HL is related to breakdown and reformation of the mesophase domains (plastic deformation of the hard domains, irreversible disruption of the microstructure, irreversible orientation, etc.) during cyclic deformation, its lowering suggests a reduction in the molecular mobility of the FF60N and VISCOPUR foams after weathering. Table 7 also reports, for all the three foams, the original values and the percent changes due to weathering exposure of 25%IFD, which denotes the surface firmness, and SF, which denotes the ability of flexible foams to support force at different indentation levels and gives an indication of cushioning quality. Again, the FF60N and VISCOPUR foams have the highest reduction in the 25%IFD values, which were already very low and typical of super-soft surfaces. The SF values slightly decrease in all cases, with a more pronounced effect for the VISCOPUR sample, indicating that the structural and

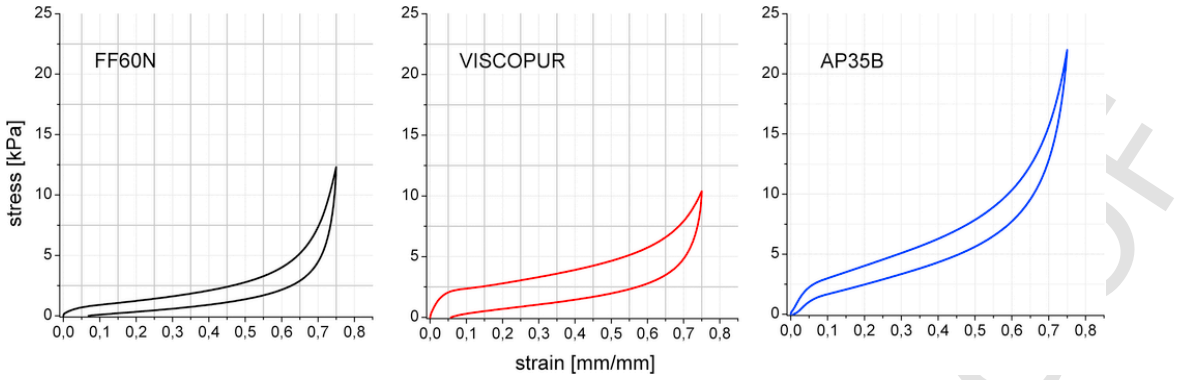

Fig. 6. Hysteresis loss curves for the FF60N, VISCOPUR and AP35B foams.

Table 5
Hysteresis loss (HL), indentation force deflection at 25% compression (25%IFD) and sag factor (SF) values of the FF60N, VISCOPUR and AP35B foam samples.

Sample	HL [%]	25%IFD [N]	SF
FF60N	48.4	6.3 ± 0.4	3.8 ± 0.3
VISCOPUR	58.4	1.9 ± 0.1	6.4 ± 0.2
AP35B	27.5	27.8 ± 0.8	2.7 ± 0.2

Table 6
Total color difference ΔE* values at different weathering times (1, 3, 6 and 12 days) for the FF60N, VISCOPUR and AP35B foams.

Sample	ΔE*			
	1 d	3 d	6 d	12 d
FF60N	1.27	1.58	2.53	3.55
VISCOPUR	1.56	3.58	4.29	5.91
AP35B	0.64	0.75	1.01	1.46

morphological changes of the foams due to weathering progressively lower their resistance to bottoming out as the load is applied and then reduce their ability to distribute body weight.

Of course, since the analyzed foams are combined in the mattress structure according to a specific layout in terms of layer order and thickness, the effects of the weathering on the comfort parameters of each layer do not directly address towards a reduction of the comfort level of the assembled mattress. Rather, they are needful data for modeling the mechanical behavior of the multi-layer mattress and predict its lifetime under specific use conditions.

4. Conclusions

In this work three flexible PU foams, used for mattress fabrication, have been tested in order to investigate the relationships among composition, morphology and some functional properties (water vapor permeability, resilience and compression mechanical behavior) of interest for their application in the bedding sector. The performed analyses evidenced that all the three foams have open cell morphology and similar cell size and distribution, but differ for their chemical structure (crosslinking degree, length of soft segments, amount and strength of the hydrogen bonds) that determines their molecular mobility. As a consequence, all systems show similar water vapor transport behavior, and thus similar breathability, which mainly depends on the foam structure, whereas strongly differ for their mechanical response. In particular, the AP35B system, which has a more rigid molecular structure, has a lower hysteresis loss, i.e. requires lower energy consumption while moving, but also a firmer surface (higher 25%IFD) and lower resistance to bottoming out (lower SF), compared to the two others, which are better able to distribute the body weight and to reduce the pressure on the body. After the artificial weathering all the foams undergo oxidation phenomena that cause color changes, perceivable also to the naked eyes, and a reduction of the molecular mobility and consequently of the mechanical parameters related to the foam comfort. The effects are more significant for the FF60N and VISCOPUR samples having lower crosslinking degree and slow recovery rate after compression: these two foams, which show a considerable decrease of both HL values (ca. 27%) and surface firmness (ca. 14–15%) and a slight decrement in their resistance to bottoming out, have proved more sensitive to weathering induced by moisture and temperature.

Acknowledgments

The authors wish to thank Dr. Stefania Rinaldi (Rinaldi Group s.r.l., Italy) for providing the foam samples used in this study.

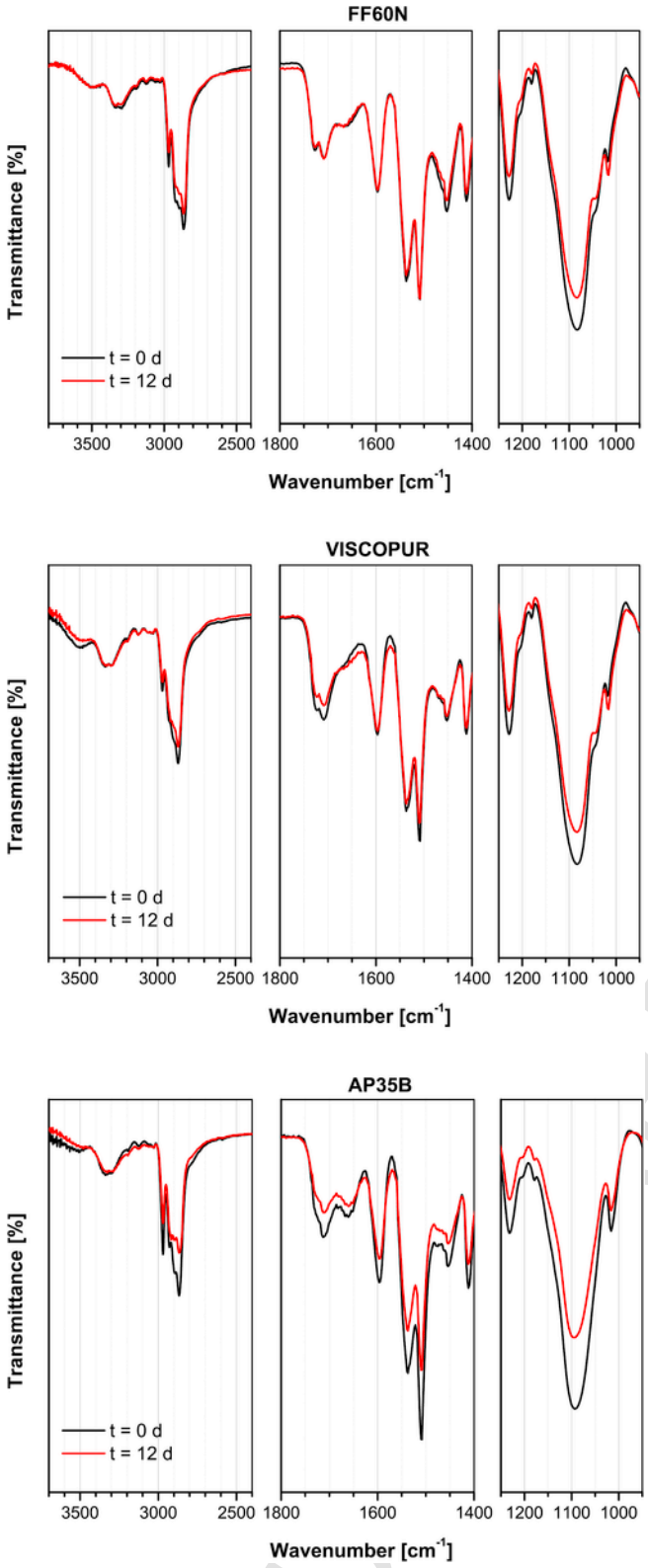

Fig. 7. Effect of weathering (T = 50 °C, R.H. = 95%) on the FT-IR spectra of the FF60N, VISCOPUR and AP35B foams.

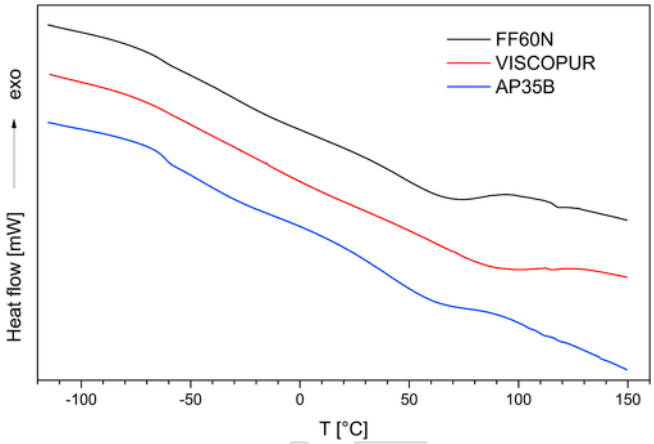

Fig. 8. Differential scanning calorimetry curves for the FF60N, VISCOPUR and AP35B foams after 12 days of artificial weathering (T = 50 °C, R.H. = 95%).

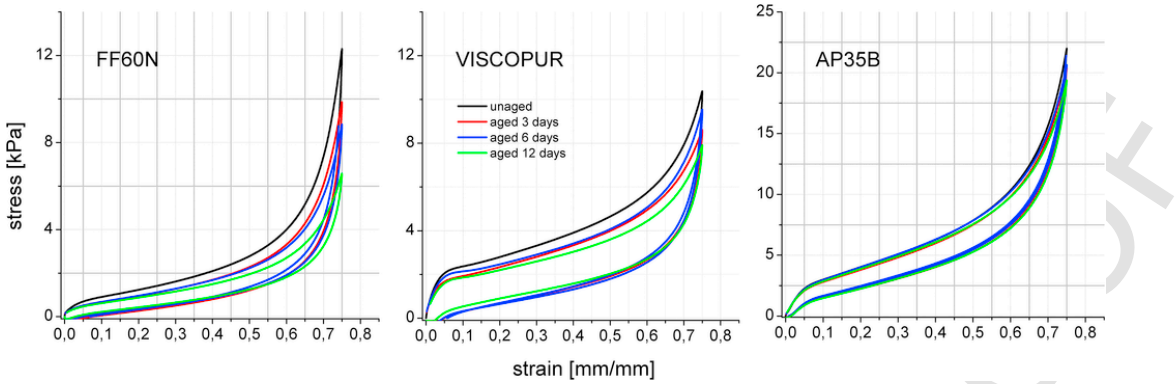

Fig. 9. Effect of weathering (T = 50 °C, R.H. = 95%) on the hysteresis loss curves for the FF60N, VISCOPUR and AP35B foams.

Table 7
Hysteresis loss (HL), 25%IFD and sag factor (SF) values of the FF60N, VISCOPUR and AP35B foams and their changes after weathering for 12 days at T = 50 °C and R.H. = 95%.

Sample	HL [%]	ΔHL [%]	25%IFD [N]	Δ 25%IFD [%]	SF	ΔSF [%]
FF60N	48.4	−27.6	6.3	−15.2	3.8	−2.9
VISCOPUR	58.4	−27.0	1.9	−13.7	6.4	−6.2
AP35B	27.5	+2.0	27.8	−8.8	2.7	−2.8

References

[1] H.-W. Engels, H.-G. Pirkl, R. Albers, R.W. Albach, J. Krause, A. Hoffmann, et al., Polyurethanes: versatile materials and sustainable problem solvers for today's challenges, Angew Chem Int Ed 52 (2013) 9422–9441.

[2] H.E. Pettermann, J. Hüsing, Modeling and simulation of relaxation in viscoelastic open cell materials and structures, Int J Solids Struct 49 (19–20) (2012) 2848–2853.

[3] B. Haex, Back and bed: ergonomic aspects of sleeping, CRC Press, Boca Raton (USA), 2005.

[4] A. Greco, F. Lionetto, The influence of the stress relaxation and creep recovery times on the viscoelastic properties of open cell foams, Polym Eng Sci 49 (2009) 1142–1150.

[5] F.-P. Chiang, Y. Ding, Size effect on stress–strain relation of neat polyurethane foam, Compos Part B-Engl 39 (1) (2008) 42–49.

[6] J. Nicholas, M. Mohamed, G.S. Dhaliwal, S. Anandan, K. Chandrashekhara, Effects of accelerated environmental aging on glass fiber reinforced thermoset polyurethane composites, Compos Part B-Engl 94 (2016) 370–378.

[7] A. Boubakri, N. Guermazi, K. Elleuch, H.F. Ayedi, Study of UV-aging of thermoplastic polyurethane material, Mat Sci Eng A-Struct 527 (7–8) (2010) 1649–1654.

[8] S.-B. Park, S.-W. Choi, J.-H. Kim, C.-S. Bang, J.-M. Lee, Effect of the blowing agent on the low-temperature mechanical properties of CO2- and HFC-245fa-blown glass-fiber-reinforced polyurethane foams, Compos Part B-Engl 93 (2016) 317–327.

[9] I. Coccorullo, L. Di Maio, S. Montesano, L. Incarnato, Theoretical and experimental study of foaming process with chain extended recycled PET, Express Polym Lett 3 (2) (2009) 84–96.

[10] P.C. Noble, B. Goode, T.A. Krouskop, B. Crisp, The influence of environmental aging upon the loadbearing properties of polyurethane foams, J Rehabil Res Dev 21 (2) (1984) 31–38.

[11] M. Morreale, M.C. Mistretta, M. Ceraulo, F.P. La Mantia, Rheological behavior under shear and non-isothermal elongational flow of biodegradable polymers for foam extrusion, J Polym Environ 22 (2014) 112–118.

[12] M. Kutz, Handbook of environmental degradation of materials, Elsevier, Oxford, 2012.

[13] D. Kockott, Techniques and mechanisms of polymer degradation and stabilization, natural and artificial weathering of polymers, Polym Degrad Stab 25 (2) (1989) 181–208.

[14] P. Scarfato, D. Acierno, P. Russo, Photooxidative weathering of biodegradable nanocomposite films containing halloysite, Polym Compos 36 (2015) 1169–1175.

[15] G. Rossi, C. Altavilla, P. Scarfato, P. Ciambelli, L. Incarnato, Durability study of transparent and flexible nanolayer barrier for photovoltaic devices, Polym Degrad Stabil 112 (2015) 160–166.

[16] V.S. Vinod, S. Varghese, B. Kuriakose, Effect of adhesion on the equilibrium swelling of natural rubber-aluminium powder composites, J Appl Polym Sci 70 (1998) 2427–2438.

[17] N.V. Schwartz, M. Bomberg, M.K. Kumaran, Water vapor transmission and moisture accumulation in polyurethane and polyisocyanurate foams, in: H.R. Trechsel, M. Bomberg (Eds.), Water vapor transmission through building materials and systems: mechanisms and measurement, American Society for Testing and Materials, Philadelphia, 1989, pp. p.63–72. ASTM STP 1039.

[18] ISO 11664–4:2008 (CIE S 014-4/E:2007) Colorimetry – Part 4: CIE 1976 L*a*b* Colour space.

[19] C. Zhang, Z. Ren, Z. Yin, H. Qian, D. Ma, Amide II and Aamide III bands in polyurethane model soft and hard segments, Polym Bull 60 (2008) 97–101.

[20] Y. Shi, X. Zhan, Z. Luo, Q. Zhang, F. Chen, J Polym Sci A Polym Chem 46 (2008) 2433–2444.

[21] E.A. Turi (Ed.), Thermal characterization of polymeric materials, Academic Press, London, 1981.

[22] S.M. Kang, S.J. Lee, B.K. Kim, Shape memory polyurethane foams, Express Polym Lett 6 (1) (2012) 63–69.

[23] D.J. Martin, G.F. Meijs, P.A. Gunatillake, S.J. McCarthy, G.M. Renwick, The effect of average soft segment length on morphology and properties of a series of polyurethane elastomers. II. SAXS-DSC annealing study, J Appl Polym Sci 64 (1997) 803–817.

[24] N.J. Hossieny, M.R. Barzegari, M. Nofar, S.H. Mahmood, C.B. Park, Crystallization of hard segment domains with the presence of butane for microcellular thermoplastic polyurethane foams, Polymer 55 (2) (2014) 651–662.

[25] S. Sami, E. Yildirim, M. Yurtsever, E. Yurtsever, E. Yilgor, I. Yilgor, et al., Understanding the influence of hydrogen bonding and diisocyanate symmetry on the morphology and properties of segmented polyurethanes and polyureas: computational and experimental study, Polymer 55 (18) (2014) 4563–4576.